PCCP

Accepted Manuscript

ROYAL SOCIETY OF CHEMISTRY

www.rsc.org/pccp

Multiwavelength excitation of photosensitizers interacting with gold nanoparticles and its impact on optical properties of their hybrid mixtures

Michał Kotkowiak, Alina Dudkowiak*

Faculty of Technical Physics Poznan University of Technology, Piotrowo 3, 60-965 Poznań, Poland

Corresponding author:

*E-mail: alina.dudkowiak@put.poznan.pl; Tel: +48 665 3181; Fax: +48 665 3178.

ABSTRACT

In a hybrid mixture of organic (dye) and inorganic (metallic nanoparticles) components, the optical properties of a dye can be easily controlled by tailoring the shape or concentration of the noble metal nanoparticles (NPs). The influence of multiexcitation (multiwavelength excitation) of photosensitizers (pheophorbide *a* and hematoporphyrin) on the interactions with pegylated Au-NPs, on the photophysical parameters of the dyes are studied. Detailed, systematic fluorescence quenching studies were performed in the mixtures of different contents of Au-NPs, and interpreted together with the results of quantum singlet oxygen yield examinations. According to the results, the fluorescences of the two dyes studied were effectively quenched in the presence of Au-NPs, mainly because of the resonance energy transfer between the donor (dye) and acceptor (Au-NPs). Stern-Volmer quenching constants determined, were by a few orders of magnitude higher than those describing the photochemical quenching process. In hybrid

mixtures analyzed, the mechanism of energy transfer between the donor and the aceptor was nanometal surface energy transfer. Furthermore, different behavior of the mixtures on excitation with the wavelengths from the Soret and Q bands of the dyes and with those corresponding to the surface plasmon resonance band of Au-NPs, was analyzed. Moreover, for certain concentrations of Au-NPs and for certain excitation wavelengths, an increase in singlet oxygen generation was observed. The results obtained indicate the significance of further studies of photosensitizers in hybrid mixtures with NPs.

1. Introduction

Because of high sensitivity and ease of detection, the methods based on fluorescence emission measurements have been recently widely applied for investigation of biological materials. The majority of such methods have been used for imagining**,** labeling, in diagnostics and or therapy, some of them permit investigation of processes *in vivo* in nanoscale.[1–4] In biological systems, one of the most important radiationless mechanisms of energy transfer is the Foerster resonance energy transfer (FRET), taking place between the molecules of dye, acting as a donor or acceptor of energy. In the hybrid systems composed of the dye molecules (donors) and noble metal nanoparticles (NPs) (acceptors), the interactions are described by the nanometal surface energy transfer (NSET).[2–5] In NSET the unfilled conductivity band in the metal particle is maintained by the dipole vectors on the surface of the metal, ready to accept the donor energy.[6] The main difference between FRET and NSET is that in the former the energy transfer depends on the distance between the donor and acceptor to minus 6 power (R^{-6}), while in the latter to minus 4 power (R^{-4}).[6,7] Dulkeith et al.[8] have been the first to present theoretical description of the dye fluorescence quenching near the metal nanoparticle. According to them, the presence of a metal nanoparticle in vicinity of the dye molecule leads to a drastic fluorescence quenching as a result of an increase in the rate constant of radiationless deactivation of the dye at the simultaneous decrease in the rate of dye's radiative deactivation.

Upon irradiation of their surface, gold and other noble metals show strong resonance in the visible range of electromagnetic radiation, generated by charge oscillations on the metal surface, i.e. the so-called surface plasmons. In the range of resonance frequencies, plasmons oscillate collectively with frequencies of incident electromagnetic waves

(localized surface plasmon resonance – LSPR), which is manifested as an intensive band in the extinction spectrum.

It has been shown that optical properties of metal nanoparticles depend mainly on their geometric shape and the surrounding medium.[9,10] For the above mentioned properties, NPs are more effective quenchers of the dye fluorescence than organic materials. Besides the biological systems in which the distance between interacting molecules is strictly controlled by adjustment of the number of DNA and RNA nucleotides,[11–15] much interest has been paid to heterogenic mixtures.[2,5,7,16–20] John et al.[5] have shown that a change in the shape of green synthetized Au-NPs changes the efficiency of energy transfer in the hybrid system of fluorescein-metal nanoparticle. Similar studies have been performed for coumarine-153, rhodamine 6G and DBPI in mixtures with gold nanoparticles.[7,18,19]

To the best of our knowledge, no data have been published on the effect of multiexcitation (multiwavelength excitation) of the photosensitizer interacting with Au-NPs on the photophysical properties of the dye, in particular on the yield of singlet oxygen generation (ϕ_Δ). As mentioned above, the hitherto publications have mainly concerned the fluorescence quenching phenomena. Besides systematic observation of radiative intramolecular processes and radiationless intermolecular processes, we determined the effect of the interactions between the dye and Au-NPs on the yield of singlet oxygen generation. Two dyes were chosen for the study, pheophorbide *a* (Pheide) and hematoporphyrin (HP), as they can be used in photodynamic therapy (PDT) and in diagnostics (PDD). The hybrid mixtures in ethanol were made by mixing a given dye with different amounts of Au-NPs (of about 15 nm in diameter and coated with PEG in the pegylation process). Applying different wavelengths from the range of

Soret band or Q band of the dye and from the LSPR band for Au-NPs, the effect of multiexcitation on the energy transfer and fluorescence emission quenching was studied. Theoretical analysis of the mixtures studied permitted relating the energy transfer between the dye and Au-NPs to the NSET mechanism. The above approach permitted also analysis of the effect of NPs concentration and the excitation wavelength on the yield of singlet oxygen generation in the hybrid systems studied.

2. Experimental

2.1. Chemicals

Tetrachloroauric acid ($HAuCl_4 \cdot H_2O$), sodium citrate ($HOC(COONa)(CH_2COONa)_2 \cdot 2H_2O$), O-[2-(3-Mercaptopropionylamino)ethyl]-O′-methylpolyethylene glycol (PEG-SH M_w 5000), 1,3-diphenylisobenzofuran (DPBF) were purchased from Sigma-Aldirch. Dyes: Pheide, HP, methylene blue (MB) and ethanol (EtOH) 99.8% H_2O free, were purchased from Frontier Scientific USA, Fluka and POCH S.A. Poland, respectively.

2.2. Synthesis of nanospheric Au particles and pegylation protocol

All chemicals were dissolved in Mili-Q ultra pure water in glass flasks treated with aqua regia. Citrate stabilized Au-NPs (~15 nm in diameter) were synthesized by adding 10 mL of 38.8 mM sodium citrate to 100 mL of 1 mM $HAuCl_4$ brought to reflux. After that, the reaction solution was cooled down and filtered through a 0.20 μm nylon filter. PEG-SH capping and EtOH transfer of Au-NPs were performed according to the procedure described earlier.[21,22] Briefly, 2.98×10^{-7} M of PEG-SH, sonicated previously for 15 min were added dropwise under stirring to 11 mL of Au-NPs (8.97×10^{-9} M). After 1 h the mixture was centrifuged twice (4000 rpm, 30 min). Finally, the supernatant was removed and the pellet was dissolved in 6 mL of EtOH. Pegylation

process ensures good solubility and aggregation resistance in EtOH due to formation of ultrathin PEG-SH layer on the Au-NPs surface.[21–23] The polymer layer formed on the 15 nm Au-NPs surface was around 7 nm thick.[22]

2.3. Absorption and fluorescence studies of Au-NPs-dye hybrid systems

The hybrid dye-Au-NPs mixtures were prepared according to the following procedure. The volume of all mixtures was kept constant and equal to 1.5 mL. The concentrations of Au-NPs capped by PEG-SH were as follows (0, 6.44, 8.58, 12.9, 14.2, 15.5, 17.2)×10^{-10} M (extinction coefficient 2.33×10^{8} $M^{-1}cm^{-1}$). The dye concentration was set at 1.58×10^{-6} M. The ratio of the contents of the dye and Au-NPs was kept constant for both dyes to get comparable results. Before the fluorescence quenching studies, absorption spectra were measured using a Varian Cary 4000 spectrometer. The fluorescence spectra of the mixtures were collected using a Hitachi F4500 fluorometer. All samples were stirred before and after each spectrum collection. The quantum yield of fluorescence of hybrid mixtures was calculated by the comparative method according to (1):

$$\phi_F = \phi_{Ref} \frac{F}{F_{Ref}} \frac{A_{Ref}}{A} \frac{n^2}{n_{Ref}^2} \times 100\%, \quad (1)$$

where: F and F_{Ref} are the areas under the fluorescence emission spectra of samples and the reference, respectively; A and A_{Ref} are the absorbance of the sample and the references at the excitation wavelength; n and n_{Ref} are the refractive indices of the solvents and references. The references were Pheide dye ($\phi_{Ref} = 28\%$)[24] or HP ($\phi_{Ref} = 7\%$)[25] dissolved in EtOH.

The dye photodynamic properties related to Φ_Δ were evaluated by using absorbance of DPBF widely used as $^1O_2$ trap which strongly absorbs light around 411 nm in EtOH.[26]

The reduction in absorbance of DPBF reflects generation of $^1O_2$. To estimate Φ_Δ, dyes MB and HP dissolved in EtOH were used as references. The mixtures of investigated (or reference) dyes were irradiated in a 1 cm path length quartz cuvette with monochromatic light by 1200 W (Oriel 66070) lamp, through a monochromator (Oriel 77200) (half-width of the band peak 10 nm). The irradiation wavelength was adjusted at the maximum of the Soret or Q absorption bands of the dyes or at LSPR of Au-NPs. The DPBF concentration was kept constant at the level of ~0.75×10^{-5} M. The reaction of DPBF with $^1O_2$ after irradiation was monitored by absorbance at 411 nm using a StellarNet Inc. Black-Comet-HR and DH-2000BAL Ocean Optics light source (200-1000 nm) and two Ocean Optics high quality optical fibers to collect absorption spectra.

3. Results and discussion

Pheide as a chlorophyll-like structure is widely used to construct hybrid structures for targeted PDT and PDD.[27,28] HP which is an iron-free derivative of heme, was the first commercial but not perfect photosensitizing substance used in clinical treatment.[29] Absorption spectra of Pheide and HP (with clearly indicated excitation wavelengths (λ_{exc}) used in this study) are shown in Fig.1a). The shape of HP and Pheide absorption spectra are typical of the porphyrin and chlorin derivative and confirm monomeric form of investigated dyes. The main intense band is the characteristic so-called Soret band, whereas the low intense bands in the long wavelength region are assigned as Q bands.

To evaluate the quality of Au-NPs synthesized, a theoretical simulation was performed applying the finite integration technique, a method implemented into CST Microwave Studio. The method used herein is described in our previous work.[30] Experimental absorption spectrum of Au-NPs in EtOH and theoretically calculated extinction cross

section spectrum (ECS) of 15 nm in diameter Au nanosphere are shown in Fig.1 b). LSPR band of Au nanospheric particles reaches a maximum at around 523 nm for both experimental and calculated spectra (black and red lines). The 4 nm shift in LSPR band, which is interpreted as a result of a change in the dielectric environment of NPs, is similar to that observed for citrate stabilized Au-NPs in aqueous solutions.[7] For all concentrations of Au-NPs used, the absorption spectra exhibited similar positions and shapes of the bands (results not shown).

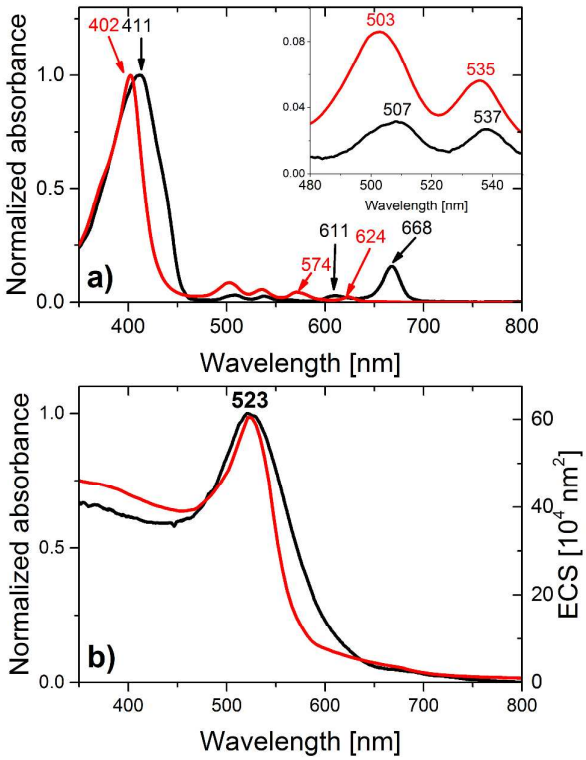

Fig. 1 Normalized absorption spectra (solid lines) of pheophorbide *a* (black line), hematoporphyrin (red line) (a), absorption (black line) and theoretically calculated extinction cross sections (red lines) spectra of Au nanoparticles (b). Additionally excitation wavelengths are indicated in (a).

Fig.2 presents the fluorescence spectra of Pheide and HP in hybrid mixtures with Au-NPs in different concentrations for λ_{exc}=507 and 503 nm, respectively. For both wavelengths, the fluorescence quenching is observed with increasing Au-NPs concentration in the mixture. The observed emission spectra of the dyes are modified due to non-radiative energy transfer between dyes and Au-NPs. The non-radiative energy transfer between donor (dye) and acceptor (Au-NPs) is a result of dynamic quenching of the fluorescence, which is observed because of diffusion interaction. In the case of static quenching, the complex in the ground state is formed which usually is a non-fluorescent product, as manifested by a new absorption band in the spectrum of the hybrid mixture or as a slight redshift of the spectrum of the donor.[31,32] Such changes were not observed for the dyes-Au-NPs mixtures studied. The last but not least quenching mechanism, which is theoretically predicted, is electron transfer, but it is noticeable if NPs diameter is lower than 5 nm.[33] Furthermore, when NPs diameter is grater than 10 nm, the fluorescence quenching takes a leading role.[34] In general, spectral overlap ($J(\lambda)$) between the absorption spectrum of the acceptor and the emission spectrum of the donor is mainly responsible for non-radiative energy transfer. The spectral overlap is calculated as follows: $J(\lambda) = \int_0^{\lambda} F(\lambda)\varepsilon(\lambda)\lambda^4 d\lambda$ $[mol^{-1}dm^3cm^3]$, where $F(\lambda)$ is normalized to the unit fluorescence spectrum, $\varepsilon(\lambda)$ is the molar extinction coefficient expressed in $mol^{-1}dm^3cm^{-1}$ at certain wavelengths λ. The value of $J(\lambda)$ is changed from 6.83×10^{-16} to 1.25×10^{-16} $mol^{-1}dm^3cm^3$ for Pheide and HP, respectively. The calculated $J(\lambda)$ values obtained in this study are not too high (so impressive) as those observed for fluorescein and cumarine 153,[7,5] however the non-radiative energy transfer is possible and observable.

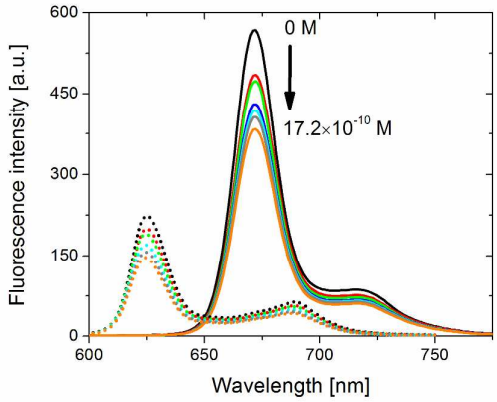

Fig. 2 Fluorescence spectra of hybrid mixtures composed of pheophorbide *a* (solid lines) or hematoporhyrin (dotted lines) with different contents of Au nanoparticles. Excitation wavelengths were 507 nm and 503 nm for pheophorbide *a* and hematoporphyrin, respectively.

A quantity that brings the information if in a given system the process of dynamic quenching dominates, is the Stern-Volmer constant, defined by the expression:[35]

$$\frac{F_0}{F} - 1 = K_{SV}[Au - NPs], \tag{2}$$

where F_0 and F are fluorescence intensities in the absence and presence of Au-NPs, respectively, K_{SV} is the Stern-Volmer quenching constant, [Au-NPs] is the concentration of NPs. The Stern-Volmer dependencies (2) for multiexcitation of Pheide and HP are shown in Fig.S1(a-b), respectively, they are linear (R^2>0.99 for both dyes). For different wavelengths of excitation (λ_{exc}) applied (which lie in different spectral regions of the absorption spectra) the character of quenching process is different. The values of K_{SV} were obtained from the slope of the plots shown in Fig.S1 and are presented in Table 1. Barazzouk et al.[32] have shown that in toluene, for a mixture of chlorophyll *a* (Chl) strongly bonded with Au-NPs, relation (2) was linear up to Au-NPs

concentration of 300 μM, while K_{SV} was 10^4 M^{-1}. The static quenching was found to be dominant in the system Chl-AuNPs. Because the K_{SV} values obtained (Table 1) are by a few orders of magnitude higher than those for the quenching process of a small dye molecule, this phenomenon is called superquenching and has been reported earlier by Ghosh et al.[7] Additionally it should be note that variability in K_{SV} values with the excitation wavelengths is not easy to observed (Table 1). Because of a high quenching coefficient of Au-NPs, their presence in very low concentrations is sufficient to strongly reduce the initial fluorescence intensity, for both types of investigated dye-Au-NPs hybrid mixtures.

A few models to describe the energy transfer between the dye and Au-NPs (donor and acceptor), have been recently proposed. Nevertheless, it has been shown that NSET provides better correlation between experimental results and theory.[5,6] In the NSET model, the distance (d_0) at which the probabilities of spontaneous emission of dye and energy transfer between dye and noble metal NPs are the same, is described by Persson-Lang surface energy equation:[6]

$$d_0 = \left(0.225 \frac{c^3 \phi_{dye}}{\omega_{dye}^2 \omega_F k_F}\right)^{1/4}, \quad (3)$$

where ϕ_{dye} is fluorescence quantum yield of the dye, ω_{dye} is the frequency of the electronic transition, ω_F and k_F are the Fermi frequency and Fermi wavevector of the metal, respectively.[6] The ϕ_{dye} is equal to 28%[24] and 7%[25] for Pheide and HP, respectively. The energy transfer efficiency (ϕ_{ET}) strongly connected with the distance between the dye and Au-NPs, is defined by:[35]

$$\phi_{ET} = 1 - \frac{F}{F_0}. \quad (4)$$

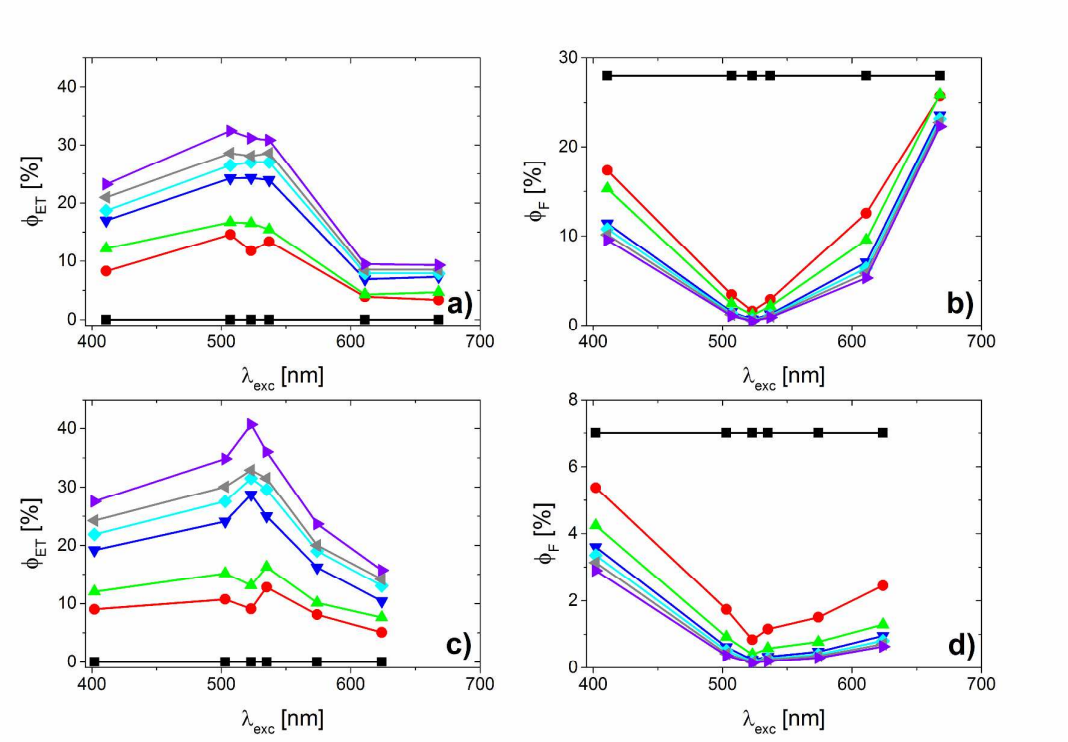

Fig. 3 The energy transfer efficiency and fluorescence quantum yield *versus* excitation wavelengths for pheophorbide *a* (a) and (b) and hematoporphyrin (c) and (d), respectively for various concentrations of Au nanoparticles. Amount of gold nanoparticles $\times 10^{-10}$ [M]: 0, 6.44, 8.58, 12.90, 14.20, 15.50, 17.20.

Fig. 3 presents the energy transfer efficiency and fluorescence quantum yield as a function of excitation wavelengths for Pheide and HP. It is interesting to point out here, that the highest ϕ_{ET} were obtained for the excitation wavelengths close to the LSPR band of Au-NPs. It is well correlated with the minimum of fluorescence emission for both dyes. However, because of a small overlap of the Pheide fluorescence and Au-NPs absorption band, the energy transfer could be difficult. However for Pheide, even at 668 nm excitation wavelength in the long wavelength region (Fig.3a) the efficiency of ET

does not drop to zero and fluorescence emission does not reach the initial yield. We could estimate that ϕ_{ET} is stabilized at the 10% level. It shows that the significant overlap of the acceptor plasmon band and the dye donor band is not a critical condition for the energy transfer between dyes and NPs in the hybrid systems investigated.

The formula which allows relating ϕ_{ET} with the distance between donor and acceptor is given by:[6]

$$\phi_{ET} = \frac{1}{1 + \left(\frac{R}{d_o}\right)^n}, \quad (5)$$

where n=4 for NSET or n=6 for FRET. Dependencies (4) and (5) can be used for Pheide and HP in the hybrid mixture with Au-NPs, the obtained results for NSET model are shown in Table S1. The experimental values of E and d_o for both Pheide and HP were used to calculate R according to (5). As a result of multiexcitation, different d_0 values were obtained (see Table 1). The experimental ϕ_{ET} as a function of R (the distance between the dye and Au-NPs) evaluated for NSET model are shown in Fig.4. The curves were simulated for n=4 and d_0 is shown in Fig.4. The obtained d_0 values shown in Fig.4 (58 Å and 41 Å for Pheide and HP, respectively) are similar to those given in Table 2 for which maximum K_{SV} values are observed (λ_{exc}=507 nm and 523 nm for Pheide and HP, respectively). A similar analysis was performed for the FRET mechanism (results not shown),[7] however the correlation between experimental results and theoretical predictions was insufficient. According to our results, for Pheide and HP dyes in a mixture with Au-NPs, the NSET mechanism is mainly responsible for the effective fluorescence quenching.

Table 1 The distance (d_0) at which the probabilities of spontaneous emission and energy transfer in the dye are the same and Stern-Volmer quenching constant K_{SV} for different excitation wavelengths (λ_{exc}), for pheophorbide *a* and hematoporphyrin.

Pheide			HP		
λ_{exc} [nm]	d_0 [Å]	$K_{SV} \times 10^8$ [$mol^{-1}dm^3$]	λ_{exc} [nm]	d_0 [Å]	$K_{SV} \times 10^8$ [$mol^{-1}dm^3$]
411	52.37	1.66	402	36.63	2.00
507	58.17	2.60	503	40.97	2.72
523	59.08	2.53	523	41.78	3.15
537	59.87	2.52	535	42.25	2.90
611	63.86	0.59	574	43.77	1.61
668	66.77	0.60	624	45.63	1.03

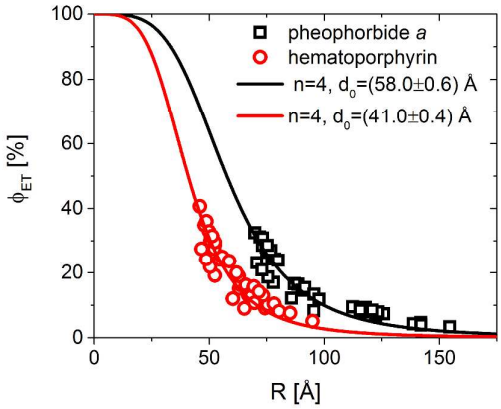

Fig. 4 Experimental energy transfer efficiency *versus* the distance between the dye and Au nanoparticles evaluated for NSET model. Graphs were fitted taking quenching data for all the excitation wavelengths presented in Table S1.

In the next step, singlet oxygen generation phenomena for Pheide and HP in the hybrid mixtures were investigated. The quenching of single oxygen by the DPBF molecule leads to its photo-oxidation. The yield of singlet oxygen generation (ϕ_Δ) is determined on the basis of the kinetics of phtotobleaching at the maximum of the absorption band at

411 nm characteristic of DPBF. On the basis of the absorption spectra recorded of irradiated samples in different time intervals, it is possible to plot the dependence of $\ln(A(0) \times A(t)^{-1})$ *versus* irradiation time, where A(0) and A(t) are absorbance values for time 0 s and for a selected moment of time, respectively. The k-rate is equal to the slope of the approximated curve and described by the equation:

$$ln\left(\frac{A(0)}{A(t)}\right) = kt. \quad (6)$$

Assuming a linear character of these dependencies, for each sample the photobleaching rate of DPBF in the presence of investigated (k_S) and reference (k_R) dyes can be evaluated. The ϕ_Δ yields were obtained according to the equation:[36,37]

$$\phi_\Delta = \phi_\Delta^R \frac{k_S}{k_R} \frac{1 - 10^{-A_R(0)}}{1 - 10^{-A_S(0)}} \times 100\%, \quad (7)$$

where $A_R(0)$ and $A_S(0)$ are absorbances of the reference and the dye investigated, respectively (for time 0). The reference ϕ_Δ^R, in the absence of Au-NPs, is 52% at 655 nm for MB, 53% at 402 nm and 505 nm for HP.[25] Exemplary plots representing kinetic curves of DPBF decay upon oxidation by reactive oxygen generated during irradiation were shown in Fig.S4. Au-NPs were found resistant to low-power-UV irradiation at room temperature, and because of this the effect their photodegradation upon ϕ_Δ determination was not taken into account.[38]

The effect of Au-NPs on the efficiency of the singlet oxygen generation, the energy transfer efficiency and fluorescence emission yield are shown, for both dyes, in Fig.5. The finally obtained ϕ_Δ values were evaluated on the basis of three independent measurements. The ϕ_Δ increased with Au-NPs concentration increasing up to ca. $5\text{-}7\times10^{-10}$ M and then decreased for excitation at Soret and LSPR bands. For higher concentration of Au-NPs, despite increase of ϕ_{ET} (and decrease of ϕ_F), the ϕ_Δ

decrease. The yields of energy transfer and fluorescence emission calculated for the selected excitation wavelengths applied take different values because of the different values of extinction coefficient of the dye (in the Soret and Q bands) and of Au-NPs (in LSPR band), but they are linear functions of the NPs concentration.

Nevertheless, more interesting behavior is observed at 668 nm excitation of Pheide. In Fig.5 we can observe a gradual increase in ϕ_Δ with increasing Au-NPs concentration. It corresponds well to the course of quenching fluorescence and energy transfer dependencies. It seems that the Pheide-NPs interaction in the region of Q_y band could be neglected, when looking for localization of NPs absorption and Pheide emission bands. However, the results suggest that the perturbation to the local electromagnetic field in the system containing Au-NPs could enhance the spin-orbit coupling, i.e. cause an increase in the probability of intersystem crossing and triplet state occupation or/and can promote the efficiency of heterogeneous triplet-triplet energy transfer. As a consequence of both above processes, the singlet oxygen generation yield increase by about 10%. Our results are consistent with that reported by Cao et al.[39] who have shown that the presence of Au-NPs enhanced the singlet oxygen generation of a dye conjugated with NPs relative to that in the system with a non-conjugated dye. The value of ϕ_Δ obtained in this study is lower than that of rose bengal (RB) dyes-Au-NPs investigated system,[39] but we have physical mixture of dyes and NPs whereas Au-NPs were conjugated with RB what influence the mechanism of ET and possibility of the photoinduced electron transfer.[32] From the results for both dyes, it is clear from Fig.5(b,d) that at the excitation at 505 nm, that is at the wavelength included both in the band of the dye and in that of LSPR, they yields of energy transfer and fluorescence quenching reach the highest values. To get a full picture of the singlet oxygen

generation phenomenon, in the hybrid mixtures, the excitation by λ_{exc}=523 nm corresponding to the Au-NPs LSPR, and to the minimum dyes' absorbances (see Fig.1 inset) was used during singlet oxygen generation studies. However, in this case, DPBF decomposition was not observed upon the irradiation of the mixtures (k values are equal to 0). On the basis of the above, we can assume that triplet states of the dyes cannot be occupied directly.

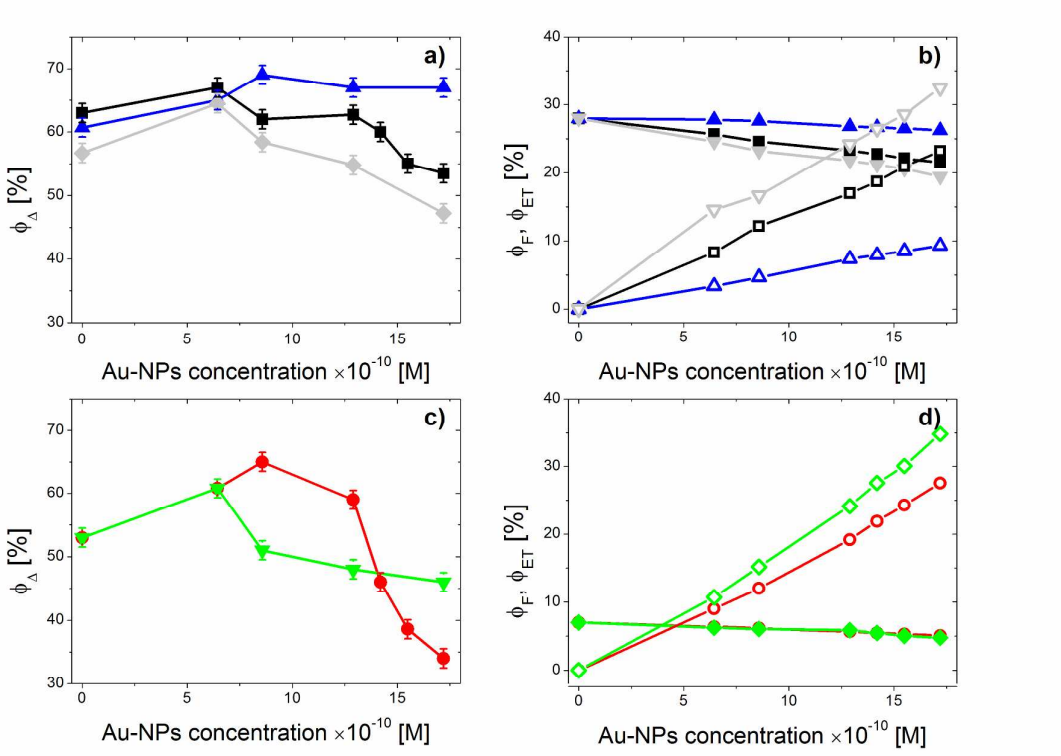

Fig. 5 The quantum yield of singlet oxygen generation (a,c), the quantum yield of fluorescence (closed symbols) and the energy transfer efficiency (opened symbols) (b,d) for dyes mixed with various concentrations of Au nanoparticles. The results were plotted for pheoprobide *a* (a,b) λ_{exc}=402 nm; 505 nm; 668 nm and black, grey and blue line, respectively, and the hematoporphyrin (c,d) λ_{exc}=402 nm, λ_{exc}=505 nm red and green line, respectively.

4. Conclusions

To sum up, there is still much to learn about the hybrid mixtures of dyes and gold nanoparticles. In this study we have shown that the interaction of the dye (the photosensitizer) and gold nanoparticles strongly affects the photophysical properties of the hybrid mixture. The superquenching observed for the hybrid mixture is mainly a result of the resonance energy transfer between the dye and the metal particle (NSET). The thin film of PEG on the surface of Au nanoparticle prevents the occurrence of the Dexter mechanism of energy transfer, moreover, the calculations excluded also the Foerster mechanism.

Our results have also evidenced different behavior of the hybrid mixtures analyzed for different excitation wavelengths, that is for the wavelengths localized in the Soret or Q band of the dye and in the range of the resonance plasmonic band of gold nanoparticles. The yields of energy transfer and fluorescence quenching were the highest for the excitation wavelength from the range of the resonance band, near 505 nm, although the absorbance of the dye at this wavelength is low. Moreover, the estimated yield of singlet oxygen generation suggests the possibility of its modification by changing the concentration of Au nanoparticles in the mixture and the amount of the energy absorbed (by adjustment of the excitation wavelength). For a mixture of Pheide-Au-NPs, the yield of singlet oxygen generation was proved to increase with the concentration of Au-NPs increasing up to about 10%, for the excitation wavelength of 668 nm. For both hybrid mixtures studied, for the other excitation wavelengths applied, the yield of singlet oxygen generation reached a maximum for Au-NPs concentrations from the range $5\text{-}7\times10^{-10}$ M. According to our results, although a small overlap of the

fluorescence band of the dye and the absorption band of Au-NPs, the presence of Au-NPs in the mixture influences the effectiveness of population of the dye triplet state and thus the effectiveness of energy transfer between the dye and molecular oxygen. Thanks to the unique photophysical properties and the possibility of control of the singlet oxygen generation and fluorescence emission, the hybrid systems studied can be applied in advanced photodynamical therapy and/or in diagnostics.

The related problem of the effect of gold nanoparticles geometry on the photochemical activity of the photosensitizers will be dealt with in a separate work.

Acknowledgements

This work was supported by the National Science Center in Poland grant number 2013/11/N/NZ7/00738.

References

1 M. Swierczewska, S. Lee and X. Chen, *Phys. Chem. Chem. Phys.*, 2011, **13**, 9929–9941.

2 R. E. Armstrong, R. A. Riskowski and G. F. Strouse, *Photochem. Photobiol.*, 2015, **91**, 732–738.

3 S. L. Raut, R. Fudala, R. Rich, R. A. Kokate, R. Chib, Z. Gryczynski and I. Gryczynski, *Nanoscale*, 2014, **6**, 2594–2597.

4 J. Zhang, C. Li, X. Zhang, S. Huo, S. Jin, F.-F. An, X. Wang, X. Xue, C. I. Okeke, G. Duan, F. Guo, X. Zhang, J. Hao, P. C. Wang, J. Zhang and X.-J. Liang, *Biomaterials*, 2015, **42**, 103–111.

5 J. John, L. Thomas, N. A. George, A. Kurian and S. D. George, *Phys. Chem.*

Chem. Phys., 2015, **17**, 15813–15821.

6 C. S. Yun, A. Javier, T. Jennings, M. Fisher, S. Hira, S. Peterson, B. Hopkins, N. O. Reich and G. F. Strouse, *J. Am. Chem. Soc.*, 2005, **127**, 3115–3119.

7 D. Ghosh, A. Girigoswami and N. Chattopadhyay, *J. Photochem. Photobiol. Chem.*, 2012, **242**, 44–50.

8 E. Dulkeith, A. C. Morteani, T. Niedereichholz, T. A. Klar, J. Feldmann, S. A. Levi, F. C. J. M. van Veggel, D. N. Reinhoudt, M. Möller and D. I. Gittins, *Phys. Rev. Lett.*, 2002, **89,** 203002-203007.

9 S. K. Ghosh and T. Pal, *Chem. Rev.*, 2007, **107**, 4797–4862.

10 J. M. McMahon, Y. Wang, L. J. Sherry, R. P. Van Duyne, L. D. Marks, S. K. Gray and G. C. Schatz, *J. Phys. Chem. C*, 2009, **113**, 2731–2735.

11 D. Sun, Y. Tian, Y. Zhang, Z. Xu, M. Y. Sfeir, M. Cotlet and O. Gang, *ACS Nano*, 2015, **9**, 5657–5665.

12 G. P. Acuna, M. Bucher, I. H. Stein, C. Steinhauer, A. Kuzyk, P. Holzmeister, R. Schreiber, A. Moroz, F. D. Stefani, T. Liedl, F. C. Simmel and P. Tinnefeld, *ACS Nano*, 2012, **6**, 3189–3195.

13 M. Jones, R. Macfarlane, B. Lee, J. Zhang, K. Yung, A. Senesi and C. Mikrin, *Nat. Mater.*, 2010, **9**, 913–917.

14 J. Chao, Y. Lin, H. Liu, L. Wang and C. Fan, *Mater. Today*, 2015, **18**, 326-335.

15 G. Rezanejade Bardajee, Z. Hooshyar and M. Khanjari, *J. Photochem. Photobiol. Chem.*, 2014, **276**, 113–121.

16 C. Banerjee, J. Kuchlyan, D. Banik, N. Kundu, A. Roy, S. Ghosh and N. Sarkar, *Phys. Chem. Chem. Phys.*, 2014, **16**, 17272–172783.

17 X. Liu, Y. Wu, S. Li, Y. Zhao, C. Yuan, M. Jia, Z. Luo, H. Fu and J. Yao, *RSC*

Adv., 2015, **5**, 30610–30616.

18 S. A. El-Daly, M. M. Rahman, K. A. Alamry and A. M. Asiri, *J. Fluoresc.*, 2015, **25**, 973–978.

19 B. R. Kumar, N. S. Basheer, A. Kurian and S. D. George, *Appl. Phys. B*, 2014, **115**, 335–342.

20 V. V. Mokashi, A. H. Gore, V. Sudarsan, M. C. Rath, S. H. Han, S. R. Patil and G. B. Kolekar, *J. Photochem. Photobiol. B*, 2012, **113**, 63–69.

21 C. Fernández-López, C. Mateo-Mateo, R. A. Álvarez-Puebla, J. Pérez-Juste, I. Pastoriza-Santos and L. M. Liz-Marzán, *Langmuir*, 2009, **25**, 13894–13899.

22 K. Rahme, L. Chen, R. G. Hobbs, M. A. Morris, C. O'Driscoll and J. D. Holmes, *RSC Adv.*, 2013, **3**, 6085–6094.

23 R. G. Shimmin, A. B. Schoch and P. V. Braun, *Langmuir*, 2004, **20**, 5613–5620.

24 I. Eichwurzel, H. Stiel and B. Roder, *J. Photochem. Photobiol. B*, 2000, **54**, 194–200.

25 M. Kotkowiak, J. Łukasiewicz and A. Dudkowiak, *Int. J. Thermophys.*, 2013, **34**, 588–596.

26 X.-F. Zhang, Q. Xi and J. Zhao, *J. Mater. Chem.*, 2010, **20**, 6726–6733.

27 I. Oh, H. S. Min, L. Li, T. H. Tran, Y. Lee, I. C. Kwon, K. Choi, K. Kim and K. M. Huh, *Biomaterials*, 2013, **34**, 6454–6463.

28 H. You, H.-E. Yoon, P.-H. Jeong, H. Ko, J.-H. Yoon and Y.-C. Kim, *Bioorg. Med. Chem.*, 2015, **23**, 1453–1462.

29 M. C. DeRosa and R. J. Crutchley, *Coord. Chem. Rev.*, 2002, **233**, 351–371.

30 M. Kotkowiak, B. Grześkiewicz, E. Robak and E. Wolarz, *J. Phys. Chem. C*, 2015, **119**, 6195–6203.

31 S. Murphy, L. Huang and P. V. Kamat, *J. Phys. Chem. C*, 2011, **115**, 22761–22769.

32 S. Barazzouk, P. V. Kamat and S. Hotchandani, *J. Phys. Chem. B*, 2005, **109**, 716–723.

33 B. I. Ipe, K. G. Thomas, S. Barazzouk, S. Hotchandani and P. V. Kamat, *J. Phys. Chem. B*, 2002, **106**, 18–21.

34 M. Li, S. K. Cushing, Q. Wang, X. Shi, L. A. Hornak, Z. Hong and N. Wu, *J. Phys. Chem. Lett.*, 2011, **2**, 2125–2129.

35 J. R. Lakowicz, *Principles of fluorescence spectroscopy*, Springer, New York, NY, 3. ed., corr. 4. print., 2010.

36 M. P. Romero, N. R. S. Gobo, K. T. de Oliveira, Y. Iamamoto, O. A. Serra and S. R. W. Louro, *J. Photochem. Photobiol. Chem.*, 2013, **253**, 22–29.

37 D. Atilla, N. Saydan, M. Durmuş, A. G. Gürek, T. Khan, A. Rück, H. Walt, T. Nyokong and V. Ahsen, *J. Photochem. Photobiol. Chem.*, 2007, **186**, 298–307.

38 Y. A. Attia, D. Buceta, F. G. Requejo, L. J. Giovanetti and M. A. López-Quintela, *Nanoscale*, 2015, **7**, 11273–11279.

39 X. Cao, B. Hu, R. Ding and P. Zhang, *Phys. Chem. Chem. Phys.*, 2015, **17**, 14479–14483.